wjpmr, 2017,3(11), 83-93

SJIF Impact Factor: 4.103

WORLD JOURNAL OF PHARMACEUTICAL AND MEDICAL RESEARCH

www.wjpmr.com

Research Article

ISSN 2455-3301

WJPMR

FLUORESCENT Mn(II) COMPLEXES OF HETEROCYCLIC SCHIFF BASES: CATALYTIC AND ANTIPROLIFERATIVE ACTIVITIES

A. K. Surabhi*[1], K. Pradeepkumar[1] and M. R. Prathapachandra Kurup[2]

[1]Research Department of Chemistry, PRNSS College, Mattanur, Kannur, Kerala, 670 702, India.
[2]Department of Applied Chemistry, Cochin University of Science and Technology, Kochi, Kerala, 682 022, India.

***Corresponding Author: A. K. Surabhi**

Research Department of Chemistry, PRNSS College, Mattanur, Kannur, Kerala, 670 702, India.

Article Received on 08/10/2017 **Article Revised on 29/10/2017** **Article Accepted on 19/11/2017**

ABSTRACT

Two novel fluorescent Schiff base ligands HL^1 and $H_2L^2.H_20$ derived from 2,6-diaminopyridine and their Mn(II) complexes were synthesized and physico-chemically characterized by means of partial elemental analyses, molar conductance measurements, magnetic susceptibility measurements and electronic, infrared, mass, EPR and ^1H NMR spectral studies. In both the complexes, two molecules of ligands are octahedrally coordinated to Mn(II) ion. HL^1 and $H_2L^2 \cdot H_20$ respectively behave as monobasic and neutral ligands in coordination with metal ion. The two complexes were given the formula $[Mn(HL^1)_2(H_20)_2]$ and $[Mn(H_2L^2)_2(OAc)_2] \cdot H_20$ respectively. The ligands and complexes exhibit enhanced blue fluorescence. The catalytic activity of these complexes was tested in the decomposition reaction of H_2O_2. These compounds show prominent anti proliferative activity.

Highlights

- Synthesis and characterization of two novel ligands and complexes.
- High thermal stability of the complexes.
- Fluorescence property.
- Catalytic activity.
- Anti proliferative activity.

KEYWORDS: Mono, bis- Schiff bases, thermal stability, catalytic activity, fluorescence, anti proliferative.

INTRODUCTION

Manganese is one of the more abundant heavy metals in the earth crust. Green plants contain fairly high concentrations of manganese and they utilize it in the oxygen evolution reaction of photosynthesis. But in animal nutrition, only trace amount of manganese is required. The elevated levels in the diet can be toxic, while the deficiency raises severe abnormalities in living tissue. These facts point out the obligatory role of manganese metalloproteins in metabolism. Manganese shows various oxidation states ranging from (-III) to (+VII). Among these, the most common and thus important is the (+II) state since Mn^{2+} ions when complexed with suitable ligand species, stable compounds, both in solid state and in solutions, are obtained.

Mn(II) complexes synthesized from heterocyclic Schiff bases, owing their air and moisture stability, low cost and facile synthesis and the ease of incorporation of required groups in the ligand structure, have assumed an important role in the field of catalysis.[1] Studies of Mn(II) complexes of pyridine based ligands have clearly demonstrated that these are versatile and effective catalysts for reactions of commercial importance like selective oxidation of hydrocarbons and cyclohexane, epoxidation of alkenes etc.[2-4] Salen based complexes of this metal ion are of great interest due to their ability to act as oxo atom transfer catalysts[5,6] and precatalysts for olefin polymerization.[7] The catalytic activity of Mn (II) complexes have been examined in the disproportionation reaction of hydrogen peroxide, low temperature peroxide bleaching of fabrics and other important reactions like hydroxylation, ring opening of epoxidation, Diels Alder reaction etc.[8-10]

Mn(II) ion is able to act as a substitute for Mg(II), the common physiological cofactor for multifarious enzymatic reactions. Many mononuclear manganese complexes are well known for their pharmaceutical uses.[11,12] Protein containing half integer, high spin Mn^{2+} complexes serve as polarizing agent for solid state dynamic polarization (DNP) of ^1H, ^{13}C, and ^{15}N at magnetic fields of 5, 9.4 and 14.1 T which will find potential applications in biophysical chemistry.[13] Numerous other applications of Mn(II) complexes have also been explored to various degrees.

Moreover, there are several specific roles for manganese in biology which have yet to be explored and elucidated. To reveal those unknown mysteries of the metal, its fluorescent molecules which can enter the cell are to be developed. Biological imaging has become a very useful tool in the field of chemical biology. This powerful tool finds potential applications in visualizing the morphology of cells and tracing the pathway and exact mechanism of intakes and release of several biological factors. It is realized that fluorescent molecules are eminently suited to facilitate such utilities and will play a vital role in this field. Fluorescence span a wide range of applications ranging from the use of fluorescent tags to detect nonfluorescent molecules, chemical derivatization to convert non fluorescent molecules to fluorescent derivatives and a method for quantification of trace elements.

The study of complexes of Schiff bases derived from pyridine derivatives are very relevant due to their potential applications in various fields. Metal complexes of Schiff bases derived from isomeric diaminopyridines acquired deep interest due to the ease of preparation, different modes of binding, availability of ring nitrogen with a lone pair and a variety of properties applicable in different fields of science. But very few studies were reported with these isomeric diaminopyridines. Earlier studies revealed the antibacterial and catalytic properties of Schiff base complexes from 2,3-diaminopyridine.[14-16] Reports have proved that metal chelates of ligands from 3,4-diaminopyridine find potential uses in drug designing.[17] The spectral and thermodynamic properties of unsymmetrical cobalt complexes of Schiff bases of 2,3-diaminopyridine and 3,4-diaminopyridine were revealed.[18] Ali et al studied the synthesis of heterocyclic Schiff base complexes of transition metal carbonyls.[19]

The importance of manganese in biological chemistry prompted us to synthesize novel fluorescent Mn(II) complexes of 2,6-diaminopyridine based ligands and herein we report their synthesis, spectral characterization, catalytic and anti proliferative properties.

EXPERIMENTAL

Materials and reagents

All the chemicals used are of analytical grade. 2,6-Diaminopyridine was purchased from Across Organics. 2-hydroxy-3-methoxybenzaldehyde and Mn(II) acetate tetrahydrate were supplied by Sigma-Aldrich. All solvents were of analytical grade and were used as such. MTT (3-(4,5-dimethylthiazol-2-yl)-2,5-diphenyl tetrazolium bromide) is purchased from Sigma. HeLa (cervical cancer) cell lines were procured from National Centre for Cell Sciences (NCCS), Pune, India.

Instruments

Elemental analyses (CHN) were performed on an Elementar Model Vario ELIII CHNS Analyser. Metal estimation was done by the standard gravimetric method. Magnetic measurements were conducted using a Sherwood Scientific model Mag way MSB MK1 magnetic susceptibility balance. Molar conductance values of the solutions of complexes in DMSO (~10^{-3}M) were obtained from a Deluxe conductivity meter, Model 601E. IR measurements of the compounds in the 4000-400cm^{-1} were carried out by the KBr pellet method using a Thermo Nicolet AVATAR 370 DTGS model FT IR Spectrophotometer. Mass spectra of the ligands and complexes were recorded in a JMS-T100LC, Accu TOF (DART-MS) mass spectrometer. Thermogravimetric analysis (TG-DTG) was performed using NETZSCH STA 449F3 JUPITER TG-DSC analyser in an atmosphere of nitrogen gas at a heating rate of 10 K/min. ^{1}H NMR spectra of the ligands were recorded using FT NMR Bruker Avance III, 400MHz model spectrophotometer with DMSO as the solvent. Solution state electronic spectral measurements of the ligands and complexes in DMSO solvent in the range 200-900 nm were carried out with the help of Systronics-2201 model spectrophotometer. X band EPR measurements were conducted in a JEOL Model JES-FA 200 spectrophotometer. Fluorescence measurements were done in a Perkin Elmer spectrofluorimeter. NBS Eppendorf incubator, Gibco invitrogen DMEM and Olympus CKX41 Microscope with Optika Pro5 CCD camera were used for *in vitro* anti-proliferative analysis.

Synthesis of Mono Schiff base ligand HL[1]

[(2E)-N2-[(3-methoxy-2-methylphenyl)methylidene]pyridine-2,6-diamine]

Ethanolic solutions of 2,6-diaminopyridine (0.109g,1mmol) and 2-hydroxy-3-methoxy benzaldehyde (0.153g,1mmol) in 1:1 ratio were refluxed for three hours and the resulting dark orange solution was allowed to stand overnight for evapouration of the solvent. The dark orange precipitate of Mono Schiff base was filtered, washed with ethanol, recrystallized from hot ethanol and dried.

Synthesis of Bis Schiff base Ligand $H_2L^2\cdot H_20$

[(1E)-1-(3-methoxy-2-methylphenyl)-N-{6-[(E)-[(3-methoxy-2-methylphenyl)methylidene]amino]pyridin-2-yl}methanimine hydrate]

2,6-diaminopyridine (0.109g,1mmol) and 2-hydroxy-3-methoxybenzaldehyde (0.304g, 2mmol) were dissolved separately in ethanol (ratio 1:2) and the latter is poured to the former with constant stirring. The mixture was refluxed for three hours and the resulting dark red solution was concentrated by evaporation. The gulmohar red precipitate of Bis Schiff base was filtered, washed with ethanol and dried.

Molecular structure of the Schiff base ligands HL^1 and $H_2L^2\cdot H_20$

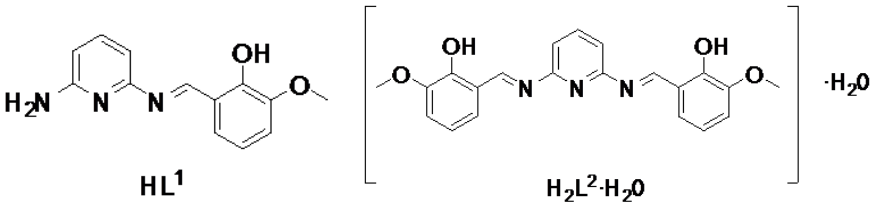

Synthesis of metal complexes

A general procedure was employed for the synthesis of both metal complexes. The Schiff base ligand was dissolved in sufficient quantity of DMF and 10 ml of ethanol was added to it. Equimolar amount of ethanolic solution of Mn(II) acetate tetrahydrate was added to the ligand. The mixture was refluxed for three hours. The refluxed solution was concentrated by evaporation and the precipitate obtained was filtered, washed successively with ethanol and ether and dried.

Catalytic activity

At room temperature, the metal complex (~ $2x10^{-6}$ M) was mixed with 50 ml of H_2O_2 (0.1 N) in a flask under constant stirring. Then, the extent of hydrogen peroxide decomposed at different intervals of time was estimated by permanganometric titration method. 5 ml aliquot of reaction mixture is withdrawn in each 30 minutes upto 4.5 hours and titrated with 0.01 M $KMnO_4$ in the presence of 0.01 M H_2SO_4. The difference in titer values of the $KMnO_4$ solution before and after the catalyzed decomposition was recorded.

In vitro Anti proliferative effect determination by MTT Assay

HeLa (cervical cancer) cell lines were maintained at Dulbecos Modified Eagles Medium (DMEM). The cell line was cultured in 25 cm^2 tissue culture flask with DMEM supplemented with 10% FBS, L-glutamine, sodium bicarbonate and antibiotic solution containing Penicillin (100 µg/mL), streptomycin (100 µg/mL) and amphoteracin B (2.5 µg/mL). Cultured cell lines were kept at 37 ℃ in a humidified 5% CO_2 incubator. The viability of cells were evaluated both by direct observation of cells by Inverted phase contrast microscope and followed by MTT assay method.

Two days old confluent monolayer of cells were trypsinized and the cells were suspended in 10% growth medium, 100µL cell suspension ($5x10^4$ cells/well) was seeded in 96 well tissue culture plate and incubated at 37 ℃ in a humidified 5% CO_2 incubator. 1mg of each sample compound was added to 1mL of DMEM and dissolved completely by cyclomixer. After that the extract solution was filtered through 0.22 µm millipore syringe filter to ensure the sterility. After 24 hours, the growth medium was removed, freshly prepared samples in 5% DMEM were serially diluted five times by two fold dilution (100µg, 50 µg, 25 µg, 12.5 µg, 6.25 µg in 100µL of 5% DMEM) and each concentration of 100µL were added in triplicates to the respective wells and incubated at 37 ℃ in a humidified 5% CO_2 incubator.

Cytotoxicity Assay by Direct Microscopic observation

Entire plate was observed at an interval of each 24 hours up to 72 hours in an inverted phase contrast tissue culture microscope and microscopic observation were recorded as images. Any detectable changes in the morphology of the cells, such as rounding or shrinking of cells, granulation or vacuolization in the cytoplasm of the cells etc were considered as indicators of cytotoxicity.

Cytotoxicity Assay by MTT Method

15 mg of MTT was reconstituted in 3 ml PBS until completely dissolved and sterilized by filter sterilization. After 24 hours of incubation period, the sample content in wells were removed and 30µL of reconstituted MTT solution was added to all test and cell control wells, the plate was gently shaken well, then incubated at 37 ℃ in a humidified 5% CO_2 incubator for 4 hours. After the incubation period, the supernatant was removed and 100µL of MTT Solubilization Solution (DMSO) was added and the wells were mixed gently by pipetting up and down, in order to solubilize the formazan crystals. The absorbance values were measured by using microplate reader at a wavelength of 570 nm. The percentage of growth inhibition was calculated using the formula

$$\text{Percentage of cell viability} = \frac{\text{Mean Optical density of sample}}{\text{Mean Optical Density of Control group}} \times 100$$

RESULTS AND DISCUSSION

The analytical and physical data of the ligands and their complexes are presented in Table 1. All the compounds are partially soluble in ethanol and completely soluble in polar organic solvents like chloroform, DMF, DMSO, etc. Both the complexes are octahedral. Mono Schiff base complex has a structure in which two anionic ligands are coordinated to the Mn(II) ion while bis Schiff base complex is formed by the coordination of two neutral ligands to the Mn(II) ion along with two acetate ions satisfying the primary valency.

Conductivity measurements of the two complexes in DMSO (10^{-3} M) indicate that these are nonelectrolytes in DMSO. The magnetic moments of the two complexes, MnL^1 and MnL^2 calculated from magnetic susceptibility measurements and using the diamagnetic corrections are 5.42 and 5.87 B.M., respectively, indicating the presence of five unpaired electrons and hence these are high spin complexes.[20,21]

Table 1: Analytical and physical data of the Schiff bases and their metal complexes.

Compound	Mp °C	M. Wt.	Colour (% yield)	C% found (calc.)	H% found (calc.)	N% found (calc.)	M% found (calc.)	μ_{eff} BM	Λ_M $Ohm^{-1}mol^{-2}cm^2$
$C_{13}H_{13}N_3O_2$ (HL^1) , L^1	130	243	Dark orange 90%	65.25 (64.5)	5.37 (4.95)	16.54 (17.3)	-	-	-
$C_{21}H_{19}N_3O_2 \cdot H_2O$ (H_2L^2)·H_2O,	160	396	Orange red 90%	63.51 (63.62)	5.18 (4.79)	10.83 (10.6)	-	-	-
$[Mn(HL^1)_2(H_20)_2]\cdot$	>300	575	Light green 84%	54.41 (54.26)	4.93 (4.86)	14.67 (14.2)	9.47 (9.56)	5.42	8.2
$[Mn(H_2L^2)_2(OAc)_2]$	>300	945	Cow dung green 89%	58.30 (59.41)	4.95 (4.86)	9.41 (8.86)	5.69 (5.9)	5.87	2.6

IR and ^{1}H NMR Spectroscopy

The infrared spectral assignments (cm^{-1}) of the ligands and their Mn(II) complexes are tabulated in Table 2. Comparison of IR spectra of complexes with that of respective ligands in the region 4000-400 cm^{-1} revealed significant variations in the charactereristic bands due to coordination with the metal ion. The infrared spectra of the ligand HL^1 showed a strong band 1611 cm^{-1} which can be due to azomethine group formed by the condensation reaction.[22] Two bands appeared at 3455 and 3205 cm^{-1} due to asymmetric and symmetric stretching vibraton of the primary amino group in the ligand molecule.[23] The spectrum of complex $[Mn(HL^1)_2(H_20)_2]$ showed appreciable shifts in the ν(C=N) of azomethine group and $\nu(C-O)$ bands without shift in the ν(C=N) of pyridine group. These results indicate that the coordination of manganese to the ligand through its oxygen of the hydroxyl group and azomethine nitrogen.[24] It can be confirmed from the fact that the medium sharp band at 3366 cm^{-1}, characteristic of –OH stretching vibration in ligand is found replaced by a strong broad band starting from 3400 to 3280 cm^{-1}. It may be due to the asymmetric and symmetric stretching vibration of water molecule present in the complex. Moreover, the complex exhibits rocking (ρ_r), twisting (ρ_t) and wagging (ρ_w) modes of coordinated water molecule at 834 cm^{-1}, 623 cm^{-1} and 500 cm^{-1}, respectively, which confirm the presence of water in the coordinated form.[25] Appearance of new bands in the spectra at 515 cm^{-1} and 403cm^{-1} can be assigned to ν M-N and ν M-O stretching vibrations.[26] From the spectral analysis, it is concluded that the octahedral coordination sphere of Mn(II) ion in complex $[Mn(HL^1)_2(H_20)_2]$ may be completed by two molecules of bidentate ligand and two water molecules.

Table 2: IR Spectral Assignments of ligands and complexes (cm^{-1}).

Compound	ν(C=N) cm^{-1}	ν(C=N) of py cm^{-1}	$\nu(O-H)$ cm^{-1}	ν(C-N) cm^{-1}	$\nu(C-Npy)$ cm^{-1}	ν(C-O) phenol cm^{-1}	$\nu(C-O)$ ether cm^{-1}	$\nu_a(COO^-)$ cm^{-1}	$\nu_s(COO^-)$ cm^{-1}	ν(M-N) cm^{-1}	ν(M-O) cm^{-1}
HL^1	A broad and strong band from 1668-1522 pointed at 1611		3366	1477, 1454	1439	1272	1220	-	-	-	-
$[Mn(HL^1)_2(H_20)_2]\cdot$	A broad and strong band from 1690-1530 pointed at 1610		3360	A broad and strong band from 1490-1390 pointed at 1450		1260	1220	-	-	515	403 (M – Ophenol
$H_2L^2\cdot H_20$	1609 (broad)	1575	3363	1452		1271	1211	-	-	-	-
$[Mn(H_2L^2)_2(OAc)_2]\cdot H_20$	1607 (asy), 1547 (sym)	1572	3355	1465	1437	1271	1213	1589	1339	448	410 (M –acetate oxygen bond)

The ^{1}H NMR spectrum of HL^1 in deuterated DMSO showed two singlets at δ 13.12 ppm (1H) and δ 6.68 ppm (2H) due to hydroxyl and amino protons. Two multiplets at δ 6.21-6.92 ppm (3H) and δ 7.01-7.42 ppm (3H) can be respectively assigned to pyridyl and phenyl protons. Azomethine proton and methyl protons are observed as singlets at δ 8.78 ppm (1H) and δ 3.83 ppm (3H). The complex is not giving NMR spectra indicating the paramagnetic nature.

The infrared spectrum of $H_2L^2\cdot H_20$ showed a strong broad band ~ 1636 to 1582 cm^{-1} which can be due to azomethine group formed by the condensation reaction (the broadness may be due to the possibility of

asymmetric and symmetric stretching vibrations of azomethine groups, formed on the second and sixth position of pyridine ring) and a sharp one ~1575 cm^{-1} due to the C=N group of pyridine moiety. The strong intramolecular hydrogen bonding between hydroxyl proton and azomethine nitrogen in the ligand lead to broad and weak hydroxyl absorption in the region 2700-2750 cm^{-1}.[27] On complexation, the frequency of asymmetric vibration of azomethine group decreases while that of symmetric vibration increases. The net effect observed was a small increase in the point of maximum transmittance while the broad band as a whole corresponded to the C=N group, shifted to lower energy[24] indicating the coordination of azomethine group to the metal ion. The IR spectrum of $[Mn(H_2L^2)_2(OAc)_2]\cdot H_20$ exhibits a band at 3372 cm^{-1} as in $H_2L^2\cdot H_20$ indicating uncoordinated fashion of –OH groups. The energy of C-O stretching vibration of phenolic part is not changed abruptly in the complex and this rules out the possibility of coordination of phenolic oxygen towards manganese ion.[28] The band for pyridyl C=N is found unchanged in position. Moreover, it is substantiated with the presence of a medium band at 777 cm^{-1} and a weak band at 730 cm^{-1}, corresponding to the out of plane(π) and in plane (δ) pyridyl ring deformation respectively, both in $H_2L^2\cdot H_20$ and $[Mn(H_2L^2)_2(OAc)_2]\cdot H_20$. The region from 1500-1100 cm^{-1} in the spectrum of ligand and complex is rich with a number of bands, which can be attributed to the C-O stretching vibration of phenol, both asymmetric and symmetric C-O-C stretching vibration of the attached methoxy group, bending vibration of methyl group, bending vibration of C-O-H, in plane and out of plane bending vibrations of –O-H group, bending vibrations of C-H bonds, etc. The coordination sphere is assumed to be formed by bonding with two azomethine nitrogens each from two ligand molecules and expected to be completed by bonding with oxygen atoms of two acetate groups. That is evident from the asymmetric and symmetric stretching bands of acetate group at 1589 and 1339 cm^{-1} in the spectrum of the complex. The difference between these bands (250 cm^{-1}) suggests the bonding of acetate groups in the unidentate fashion.[26] The non-ligand bands in between 500-400 cm^{-1} can be assigned to the Mn-N and Mn-O bonds.

The signals observed in the ^1H NMR spectrum of $H_2L^2\cdot H_20$ in deuterated DMSO is in accordance with the proposed structure. It showed one singlet at δ 10.273 ppm (2H) due to hydroxyl proton. The strong intramolecular hydrogen bonding may be responsible for the upfielded signal.[23] The two multiplets observed at δ 7.269 - 7.244 (6H) and δ 6.944-6.905 ppm (3H) can be attributed to the phenyl protons and pyridyl protons respectively.[19] The spectrum revealed a singlet at δ 7.125 ppm (2H) that can be assigned to the azomethine proton. Two singlets at δ 3.855 (3H) and 3.811 ppm (3H) corresponds to the two sets of methyl protons. A singlet at δ 3.797 ppm (2H) provides evidence for H_2O protons.[29] The complex is silent in the radio frequency field and hence the paramagnetic nature is confirmed.

Mass Spectra

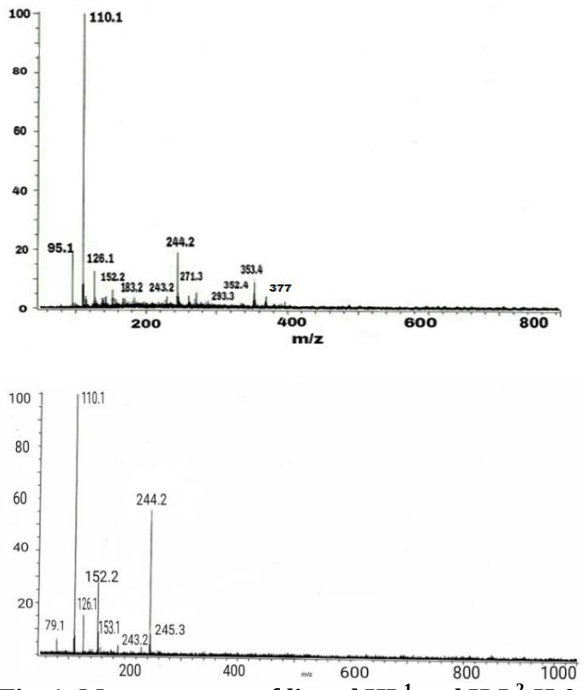

Fig. 1: Mass spectrum of ligand HL^1 and $H_2L^2\cdot H_20$.

Mass spectrometry is considered as an excellent tool for getting the molar mass and the mode of fragmentation gives the exact structure of the compounds. The characteristic fragments can be given as m/z (%). The molecular ion peak of HL^1 is observed at 243 (8) amu (calc.243). [(M+1) peak is found at 244(59) with greater intensity]. The ion peak at 211 corresponds to the species $[C_{12}H_9N_3O]^+$. Peak at 152 (30) amu (calc.152) stands for 2-hydroxy-3-methoxybenzaldehyde molecule and the base peak is obtained at 110 (100) amu (calc.109), indicating the formation of 2,6-diaminopyridine molecule. Finally the formation of pyridine molecule is confirmed by the peak at 79 (8) amu (calc.79). The mass spectrum of the ligand is given (Fig. 1).

The molecular ion peak of $H_2L^2\cdot H_20$ is observed at 377 (5) amu (calc.395) although the relative intensity is very small after removing the water molecule. The spectrum exhibits peaks at 369 (5) amu (calc.368) and 353 (13) amu (calc.353), corresponding to the removal of $CH_2=CH_2$ and CH_3-$CH=CH_2$, respectively, from one of the 2-hydroxy-3-methoxybenzaldehyde moieties. The species formed by the removal of one molecule of 2-hydroxy-3-methoxybenzaldehyde as a whole was indicated by the peak at 244 (20) amu (calc.243). The mass spectra showed the base peak at 110 (100) amu (calc.109) corresponding to the species 2,6-diaminopyridine.

The mass spectrum of the complex, $[Mn(HL^1)_2(H_20)_2]$ exhibits a peak at 575 (5) amu (calc.575) which represents the molecular ion peak. The existence of the

ligand is revealed by the peak at 243 (15) amu (calc.243). The peak observed at 492 (8) amu and 391.5 (8) amu can be referred to as the removal of some groups of ligand molecules. The removal of one ligand molecule is indicated by the peak at 293 (10) amu (calc.295). The fragmentation of the ligand molecule gives the peaks at 171 (20) amu (calc.171) and 153(20) amu (calc.152) which can be assigned to the hydrated molecule of 2-hydroxy-3-methoxybenzaldehyde and anhydrous molecule of 2-hydroxy-3-methoxybenzaldehyde. Finally the base peak is found at 79 (100) amu (calc.79) indicating the formation of pyridine molecule.

The molecular ion peak of the complex, $[Mn(H_2L^2)_2(OAc)_2]\cdot H_20$ is observed at 925 (10) amu (calc.927) excluding the water molecule. The existence of ligand molecule is indicated by the peak at 391 (20) amu (calc.396). The mass spectrum exhibits peaks at 882, 842, 808, 734, 663, 635, 594, 471 and 411 with relative intensity less than 10 indicating the formation of several unstable intermediates by the removal of typical groups or parts of the ligand. The ligand molecule undergoes further fragmentation to produce the base peak at 157 (100) amu (calc.153) corresponding to 2-hydroxy-3-methoxybenzaldehyde and finally the peak at 79 (70) amu (calc.79) corresponding to pyridine molecule.

Electronic spectra

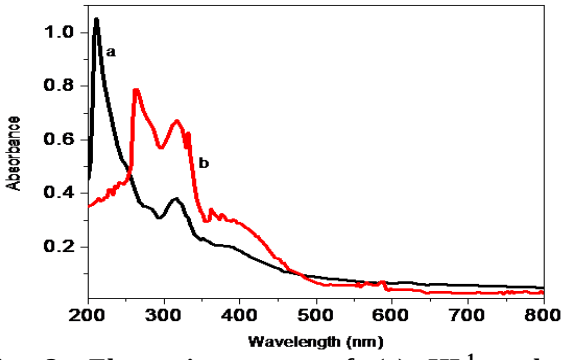

Fig. 2: Electronic spectra of (a) HL^1 and (b) $[Mn(HL^1)_2(H_20)_2]$ in DMSO.

For high spin octahedrally coordinated Mn(II) complexes with d^5 configuration, the ground state is ^6A_1g. There are no other terms of sextet spin multiplicity and hence there are no spin allowed d-d transitions. The absorption intensities of manganese complexes are extremely low because of the doubly prohibition involving the Laporte rule and spin multiplicity rule.[30] The d^5 configuraton give rise to ^4G, ^4P, ^4D as the quartet terms, of which ^4G lies as the lowest excited state consistent with the Hund's rule. In an octahedral field among the possible energy bands, the three lowest are assigned to $^4T_{1g}(G) \leftarrow {}^6A_{1g}$, $^4T_{2g}(G) \leftarrow {}^6A_{1g}$ and $^4E_g(G), {}^4A_{1g}(G) \leftarrow {}^6A_{1g}$ transitions. The pair of transitions $^4E_g(G), {}^4A_{1g}(G) \leftarrow {}^6A_{1g}$ are degenerate whose energies are given by $10B+5C$. These assignments are obtained by fitting the observed spectrum to the Tanabe Sugano diagram.[31] Both the complexes exhibit three weak absorption bands at ca. 17000, 21000 and 25000 cm^{-1} (Fig. 2). The energies corresponding to the observed absorption bands of the two ligands and their Mn(II) complexes are listed in Table 3.

The values of Racah parameters B and C and Dq calculated for the complexes are also given. The extent of delocalization of metal electrons can be evaluated from the electronic spectrum by estimating $\beta = B/B_0$. The value of B_0 for Mn^{2+} ion is 860 cm^{-1}[32] The absorption bands observed for $n \rightarrow \pi^*$ and $\pi \rightarrow \pi^*$ transitions of the ligands are slightly shifted in the complexes.

Table 3: Electronic spectral data of Mn(II) complexes (cm^{-1}).

Compound	$^4T_{1g}(G) \leftarrow {}^6A_{1g}$	$^4T_{2g}(G) \leftarrow {}^6A_{1g}$	$^4E_g(G), {}^4A_{1g}(G) \leftarrow {}^6A_{1g}$	$n \rightarrow \pi^*$	$\pi \rightarrow \pi^*$	B	10Dq	C	$\beta = \frac{B}{B_0}$
HL^1	-	-	-	31545	47393				
$[Mn(HL^1)_2(H_20)_2]$	16977	25641	26595	30211 27624	38314	642	9641	2828	0.7465
$H_2L^2\cdot H_20$	-	-	-	34965 29173	42372				
$[Mn(H_2L^2)_2(OAc)_2]\cdot H_20$	16583	20833	23310	37453 29411	37452	631	7935	2779	0.7348

EPR Spectra

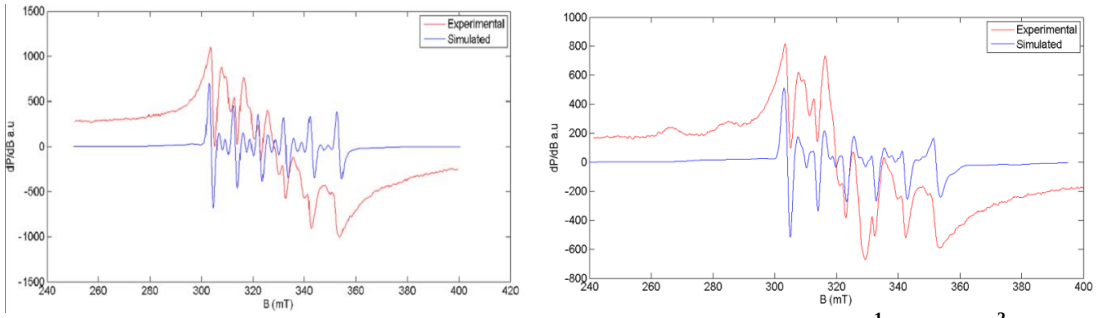

Fig. 3: Simulated and experimental best fits of EPR spectra of the complexes MnL^1 and MnL^2 respectively.

The electron spin properties of manganese compounds provide better understanding about Mn ion centers. The Mn(II) ion centers in complexes possesses Kramers' ground-state doublets and exhibits characteristic spin transitions in the normal mode X-band regime. The spin Hamiltonian used to represent Mn(II) is given by

$$H = g\beta BS + IAS + D\left[S_2^2 - \frac{S(S+1)}{3}\right] + E(S_x^2 - S_y^2)$$

where B is the magnetic field vector, g is the spectroscopic splitting factor, β is the Bohr Magneton, D is the axial zero field splitting parameter, E is rhombic zero field splitting parameter and S is the electron spin vector. The first two terms represent the electronic Zeeman and the electron nuclear hyperfine interactions, respectively, whereas the last two terms define the zero-field splitting interaction with D and E gauging the axial and the rhombic parts.[33] The solid state EPR spectra of both the complexes at room temperature are characterized by broad signals as a result of dipolar interactions and random orientation of Mn^{2+} ions.[34] The frozen solution spectra for both Mn(II) complexes were simulated using EasySpin.[35] The solution spectra of both compounds in DMSO at 77K were almost similar exhibiting a six line hyperfine pattern, centered at g =1.978 and 1.976, for complexes MnL^1 and MnL^2 respectively. This is expected for an odd unpaired electron system with S = ±5/2, M_S = ±5/2, ±3/2, ±1/2 and I = ±5/2, M_I= ±5/2, ±3/2, ±1/2 with g and A tensors isotropic, resulting from allowed transitions (Δm_S= ± I, Δm_I = 0). The six hyperfine lines are due to the interaction of electron spin with the nuclear spin (^{55}Mn, I=5/2). The observed g values are close to the free electron spin value of 2.0023 which is consistent with the typical Manganese (II) and also suggestive of the absence of spin orbit coupling in the ground $^6A_1$ state. In addition to this, a pair of low intensity forbidden lines lying between each of the main hyperfine lines is observed in the frozen solution spectra of the complexes. These forbidden lines in the spectrum arise due to the mixing of nuclear hyperfine levels by the zero field splitting factor of the Hamiltonian.[36] The ^{55}Mn hyperfine coupling constant for the complexes are estimated to be A= 264 and 274 MHz respectively. The A_{iso} values observed are lower than those of the pure ionic compounds and are consistent with the octahedral coordination.[37] For the complex $[Mn(HL^1)_2(H_20)_2]$, axial splitting factor D and rhombic splitting factor E are found to be 380 and 140 MHz respectively while those for $[Mn(H_2L^2)_2(OAc)_2]\cdot H_20$ are 280 and 80 MHz, respectively. The value for E/D ratio, calculated respectively for $[Mn(HL^1)_2(H_20)_2]$ and $[Mn(H_2L^2)_2(OAc)_2]\cdot H_20$ are 0.3684 and 0.2857. The simulated and experimental EPR spectra of the two complexes are given in Fig. 2. Based on the spectral studies, an octahedral structure can be assigned to both the Mn(II) complexes.[38]

Thermal Analysis (TG and DTG)

The structure of the complexes can be confirmed to a greater extent by thermal analysis. The nature of thermal decomposition of the compounds was studied by thermogravimetric and differential thermogravimetric techniques in an atmosphere of nitrogen gas. The results are in agreement with the proposed structure of the complexes. It is clear from the decomposition peaks that the compounds show high thermal stability. The TGA curve of complex $[Mn(HL^1)_2(H_20)_2]$ shows that the decomposition proceeds in four thermal steps. The first step of decomposition, ranges from 70-182 ℃, corresponds to a mass loss of 5.8% (calc. 6.2%). The percentage loss is consistent with the eliminaton of two molecules of lattice water. The second decomposition peak observes in the range 182- 272 ℃ with a weight loss of 16.43% (calc. 16.5%) due to loss of one molecule of aminopyridine. The peak at the temperature range 272 -800 ℃ with a weight loss 38.53% (calc. 37.4%) comprises of the third stage. It is in agreement with the loss of one ligand molecule. The final stage of decomposition up to the temperature 1400 ℃, involves 19.48% weight loss and a residual mass of 19.73% indicates that the decomposition process is not completed and above this temperature is beyond the scope of the instrument.

The complex $[Mn(H_2L^2)_2(OAc)_2]\cdot H_20$ displayed four decomposition steps when thermal decomposition is studied and thermogram is plotted up to temperature 1400 ℃. The first step is noted in the temperature range 73-258℃ with a mass loss of 14.44% (calc.14.7%), assigned to the loss of one water molecule and two acetate groups. The second step from 258-390 ℃ with a

weight loss of 15.05% (calc.14.77%) can be attributed to the removal of the aldehyde part of the ligand molecule. Next stage ranges from 390-780 ℃ and recorded a mass loss of 18.79%. It may be due to the elimination of the remaining parts one of the molecules of the ligand. Fourth step decomposition occur at 780-1150 ℃ with a mass loss of 14.35% (calc.14.77%) due to the loss of aldehyde part of the second ligand molecule. After the loss of 9.58% mass in the last stage of decomposition that we were able to conduct, a residual mass of 30.79% is observed even at 1329 ℃ indicating that decomposition process is not completed and experiment above this temperature is beyond the scope of the instrument.

Kinetic data

The kinetic parameters of decomposition processes of metal complexes were evaluated graphically from Coats–Redfern Relation.[39] The values of activation energy (E*), enthalpy (H*), entropy (S*) and Gibb's free energy (G*) were obtained for different decomposition stages graphically by employing the relation

$$\log\left[\frac{\log(W_\infty/(W_\infty - W))}{T^2}\right] = \log\left[\frac{AR}{\emptyset E^*}\left(1-\frac{2RT}{E^*}\right)\right] - \frac{E^*}{2.303RT}, \quad (1)$$

where W_∞ is the mass loss at the completion of decomposition reaction, W is the mass loss up to temperature T, R is the gas constant and ϕ is the heating rate. Since 1-2RT/E*≅1, the plot of the left hand side of the above equation against temperature will be a straight line. From the slope and the intercept, respectively, activation energy (E*) and the Arrhenius constant A can be calculated. The other parameters such as enthalpy (H*), entropy (S*) and Gibb's free energy (G*) were obtained for different decomposition stages from the following equations and the values are given in Table 4.

$$S^* = 2.303\,R\log\frac{Ah}{KT}$$

$$H^* = E^* - RT$$

$$G^* = H^* - TS^*$$

where K is the the Boltzmann and h, the Planck's constant. The high values of activation energies of decomposition indicate the high thermal stability of the investigated complexes.[40] The negative values of S* reveals the formation of more ordered activated complexes than the reactants in the slow thermal degradation reaction.[41]

Table 4: The thermodynamic data of the decomposition of the complexes.

Complex	Decomposition range(℃)	E*/kJmol^{-1}	A(S^{-1})	S*/K^{-1}Jmol^{-1}	H*/ kJmol^{-1}	G*/ kJmol^{-1}
$[Mn(HL^1)_2(H_20)_2]$	40-132	50.66	1.71×10^2	-190.82	50.02	14.51
	132-272	71.39	9.16×10	-204.34	69.66	42.57
	272-800	94.79	2.02×10^2	-203.93	91.18	88.82
$[Mn(H_2L^2)_2(OAc)_2]\cdot H_20$	33-158	42.35	1.87×10^2	-191.12	41.63	16.48
	158-280	54.13	5.82×10	-209.36	52.12	50.51
	280-490	62.83	2.21×10^2	-201.62	59.84	72.44
	490-780	67.28	6.23×10	-218.68	61.50	152.04

Catalytic activity

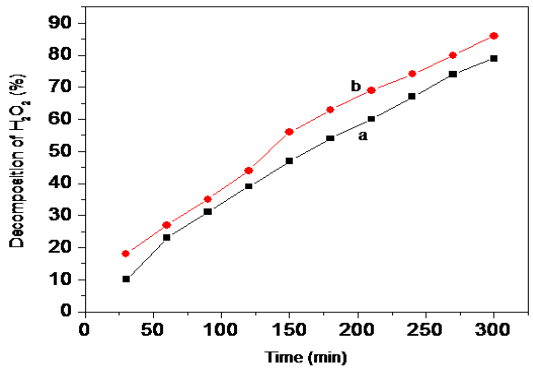

Fig. 4: The extent of decomposition of H_2O_2 (%) with time in presence of (a) $[Mn(HL^1)_2(H_20)_2]$ and (b) $[Mn(H_2L^2)_2(OAc)_2]\cdot H_20$.

The catalytic activity of the complexes was investigated by taking the decomposition of hydrogen peroxide at constant concentration as the model reaction.[42,43] The ability of two metal complexes to catalyze the decomposition of H_2O_2 has been determined by titrating the undecomposed H_2O_2 with standard $KMnO_4$ solution. The experiment is conducted with constant concentration of hydrogen peroxide (0.05 M). The percentage of H_2O_2 decomposition is found increased with time (Fig. 4). The observations are listed in Table 5. The mechanism of the catalytic decomposition of H_2O_2 as proposed in the literature[44] can be given in the following steps (1-3). Metal complex interact with HO_2^- formed by the decomposition of hydrogen peroxide to form an intermediate complex. The intermediate species react with another H_2O_2 molecule and the following products are formed.

$$H_2O_2 \rightarrow HO_2^- + H^+ \quad \ldots\ldots\ldots\ldots (1)$$

$$M\text{-}L + HO_2^- \rightarrow [ML(HO_2)]^- \quad \ldots\ldots\ldots\ldots (2)$$

$$[ML(HO_2)]^- + H_2O_2 \rightarrow M\text{-}L + H_20 + OH^- + O_2 \quad \ldots\ldots 3$$

Results show that the complexes exhibit better catalytic activity. After 4hours, 74-86% decomposition of

hydrogen peroxide can be carried out with these complexes.

Table 5: Concentration of the complexes and % decomposition of H_2O_2 at constant concentration of H_2O_2 (0.05M) at 25°C.

Compound	Concentration of complex (M)	% Decomposition of H_2O_2
$[Mn(HL^1)_2(H_20)_2]$	2.8×10^{-6}	74
$[Mn(H_2L^2)_2(OAc)_2]\cdot H_20$	3.3×10^{-6}	86

Fluorescence Measurements

Table 6: Fluorescence data of the Schiff base ligands and their metal complexes.

Compound	$\lambda_{excitation}$	$\lambda_{emission}$	Stoke's shift
HL^1	314	446	132
$H_2L^2\cdot H_20$	324	482	158
$[Mn(HL^1)_2(H_20)_2]$	320	435.5	115.5
$[Mn(H_2L^2)_2(OAc)_2]\cdot H_20$	318	436.5	118.5

The fluorescence properties of the compounds were studied at room temperature in DMSO solution (10^{-4} M) using a spectrofluorimeter keeping the exciting radiation constant. The spectral distribution of the emitted radiation is measured and the intensity versus wavelength graph is plotted to get the fluorescence spectrum (Fig. 5). HL^1 and $H_2L^2\cdot H_20$ displayed maximum emission bands at 446 nm and 482 nm respectively when excited at 314 nm and 324 nm respectively. The emission of $[Mn(HL^1)_2(H_20)_2]$ is blue shifted to 435.5nm and the emission intensity is increased compared to the ligand. The increase in intensity may be due to the extension of conjugated π electron system.[45,46] The wavelength of maximum emission in the case of $[Mn(H_2L^2)_2(OAc)_2]\cdot H_20$ is observed at 436.5nm, which also displays a blue shift compared to the respective ligand, with a reduction in intensity. The occurrence of less intense band in the complex may be due to the presence of some structural group like acetate group with quenching effect[47] which is absent in $[Mn(HL^1)_2(H_20)_2]$. The fluorescence data of the ligands and complexes with the Stoke's shift observed are given (Table 6). The enhancement of intensity through complexation in $[Mn(HL^1)_2(H_20)_2]$ and the shift in emission wavelength towards blue wavelength in $[Mn(H_2L^2)_2(OAc)_2]\cdot H_20$ is of very importance as it put forward a variety of potential applications like biological imaging, DNA sequencing etc.

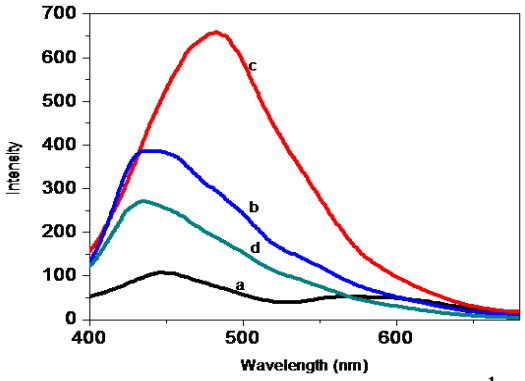

Fig. 5: Emission spectra of (a) L^1, (b) $[Mn(HL^1)_2(H_20)_2]$, (c) $H_2L^2\cdot H_20$ and (d) $[Mn(H_2L^2)_2(OAc)_2]\cdot H_20$.

Anti proliferative Activity

The two ligands and their Manganese complexes were tested for anti proliferative activity by MTT Assay method.[48] The experiments has been conducted with four different concentrations (6.5, 12.5, 25, 50 and 100 µg/mL) after serial dilution of the main stock solution. The percentage of cell viability was calculated for each sample and for each concentration. The ligand $HL^2\cdot H_20$ displayed an enhanced anti proliferative effect among the four compounds (Fig. 6). The complexes showed lesser activity than that of their ligands. $HL^2\cdot H_20$ exhibited maximum efficiency at a concentration of 100 µg/mL (Fig. 7). The microscopic image of the $HL^2\cdot H_20$ at the tested five concentrations and that of the control are given in Fig.8. The LD_{50} value (minimum concentration of the sample to be added to have a 50% cell death) calculated for it equals 67.64µg/ml.

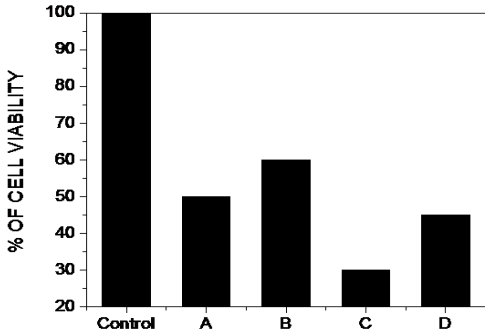

Fig. 6: The antiproliferative nature of the compounds compared to the control.
(A) L^1, (B) $[Mn(HL^1)_2(H_20)_2]$,
(C) $H_2L^2\cdot H_20$ and (D) $[Mn(H_2L^2)_2(OAc)_2]\cdot H_20$

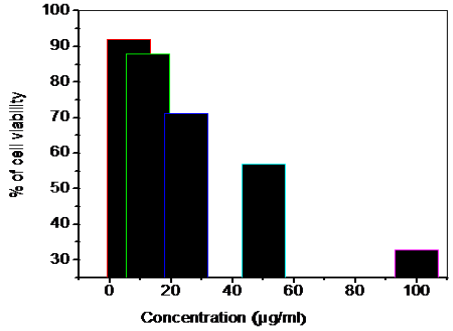

Fig. 7: Activity of $H_2L^2\cdot H_20$ at various Concentrations.

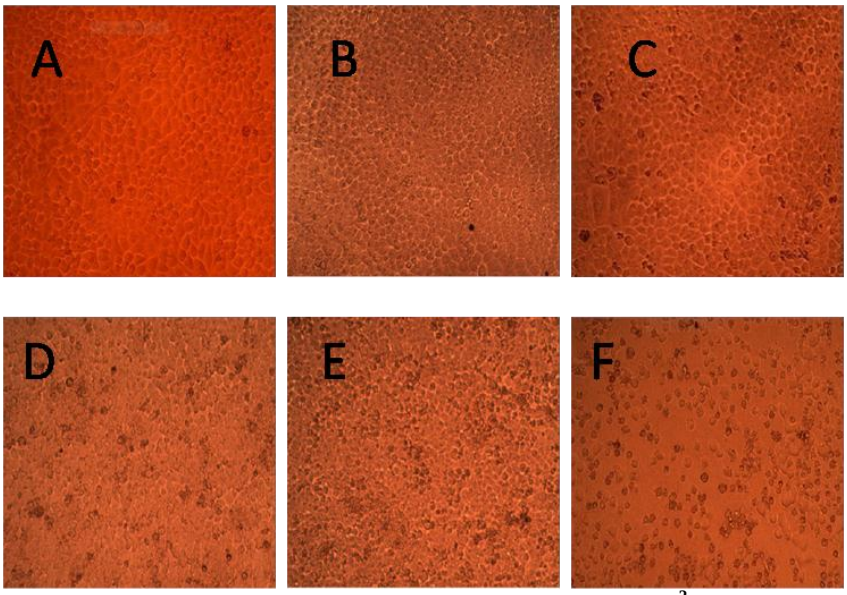

Fig. 8: Microscopic image of the anti proliferative nature of the ligand $H_2L^2 \cdot H_20$ in the order of increasing concentration. (A) Control, (B) 6.5µg/mL, (C) 12.5µg/mL, (D) 25µg/mL, (E) 50µg/mL, (F) 100µg/mL.

CONCLUSION

The synthesis and characterization of two new Schiff bases derived from 2,6-diaminopyridine and their octahedral manganese complexes were performed. Thermodynamic parameters of these complexes calculated from thermogravimetric analysis showed high thermal stability. The ligands and complexes showed intense blue fluorescence. Both the two complexes displayed good catalytic activity towards the decomposition of hydrogen peroxide and hence proved its utility as a heterogeneous catalyst. The synthesized ligands and complexes exhibited significant anti proliferative activity, among which, the ligand $H_2L^2 \cdot H_20$ showed more prominent activity with a LD_{50} value of 67.64µg/ml. The proposed molecular structures of the two complexes are given in Fig. 9.

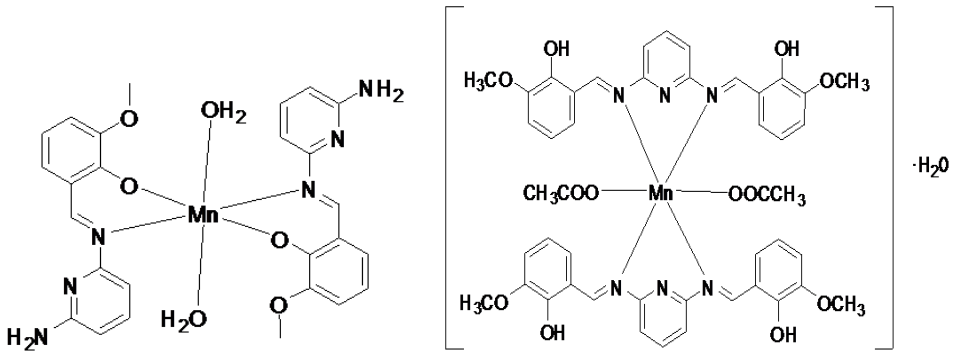

$[Mn(HL^1)_2(H_20)_2]$ $[Mn(H_2L^2)_2(OAc)_2] \cdot H_20$

Fig. 9: Molecular structures of complexes, (a) $[Mn(HL^1)_2(H_20)_2]$ and (b) $[Mn(H_2L^2)_2(OAc)_2] \cdot H_20$

ACKNOWLEDGEMENT

The authors are thankful to Sophisticated Analytical Instrument Facility (SAIF), IIT, Bombay, India, SAIF, IIT, Madras, India and SAIF, Kochi, India for the analysis. Surabhi is grateful to department of Biochemistry, Central University of Kerala for having fluorescent spectral analyses.

REFERENCES

1. P.G. Cozzi, Chem. Soc. Rev, 2004; 33: 410.
2. D.E. De Vos, P.P. Knops-Gerrits, D.L. Vanoppen, P.A. Jacobs, Supramol. Chem, 1995; 6(1/2): 49.
3. S.R. Thomas, K.D. Janla, J. Am. Chem. Soc, 2000; 122, 6929.
4. D. Chatterjee, A. Mitra, J. Mol. Catal. A. Chem, 1999; 144; 363.
5. S.Schoumaker, O.Hamelin, J.Pecant, M.Fontecare, Inorg. Chem, 2003; 42: 8110.
6. M.Louloudi, V.Nastopoulos, S.Gourbatsis, S.P.Perlepes, N.Hadjiliadis, Inog. Chem Commun, 1999; 2: 479.
7. K.Yliheikkila, K.Axenov, M.T. Raisanen, M. Klinga, M.P. Lankinen, M. Kettunen, M. Leskela, T. Repo, Organometallics, 2007; 26: 980.

8. M. Pick, I. Roboni, J.Fridovich, J. Am. Chem.Soc, 1974; 96: 7329.
9. D. Kumar, E. Derat, A.M. Khenkin, R. Neuman, S. Shaik, J. Am. Chem. Soc, 2005; 127: 17712.
10. T. Fukuda, T. Katsuki, Tetrahedron, 1997; 53: 7201.
11. G.C. Dismuker, Chem. Rev, 1996; 96: 2909.
12. R.F. Pasternack, A. Banth, J. M. Pasternack, C.S. Johnson, J. Inorg. Biochem, 1981; 15: 261.
13. M. Kaushik, T. Bahrenberg, T.V. Can, M.A. Caporini, R. Silvers, J. Heiliger, A.A. Smith, H. Schwalbe, R.G. Griffin, B. Corzilius, Phys.Chem. Chem. Phys., (2016) DOI: 10.1039/C6CPO4623A.
14. Z. Cimermann, N.Galic, B. Bosner, Anal.Chim.Acta, 1997; 343: 145.
15. T. Jeevoth, M.G. Bhowon, H.Li Kam Wah, Trans. Met. Chem, 1999; 24: 445.
16. T. Jeevoth, H. Li Kam Wah, M.G. Bhowon, D.Ghoorohoo, K. Babooram, Synth. React.Inorg.Met. Org. Chem, 2000; 6.
17. L. Flet, E. Polard, O. Guillard, E. Leray, H. Allain, L. Javaudin, G. Edan, J. Neurol, 2010; 257: 937-946.
18. M. Asadi, S. Torabi, K.Mohammadi, Spectrochimica Acta Part A.Molecular and Biomolecular Spectroscopy, 2014; 122: 676-681.
19. O.A.M. Ali, S.M. El-Medani, D. A. Ahmed, D.A. Nassar, J. Mol. Struct, 2014; 1074: 713-722.
20. B.N. Figgis, Introduction to Ligand Fields, Wiley Eastern Limited, New Delhi.
21. B.N. Figgis, J. Lewis, Prog. Inorg. Chem, 1964; 6: 37.
22. G.C. Pearcy, D.A. Thornton, J. Inorg. Nucl. Chem, 1972; 34: 3357.
23. D.L.Pavia, G.M. Lampman, G.S. Kriz, Introduction to Spectroscopy, third edition, Washington, 2001.
24. M. Mohan, P. Sharma, Inorg. Chim. Acta, 1985; 106: 197.
25. J.J. Charette, Spectrochem. Acta., 1963; 19: 1275.
26. K. Nakamoto, Infrared and RamanSpectra of Inorganic and Coordination Compounds, sixth edition,Wiley, Newyork, 2009.
27. Z. Cimermann, N. Galesic, B. Bosner, J. Mol. Struct, 1992; 274: 131.
28. M.R. Mahmoud, M.T.El. Haty, J. Inorg. Nucl.Chem, 1980; 42: 349.
29. S. Ilhan, H.Temel, I. Yilmaz, M. Sekerci, Polyhedron, 2007; 26: 2795.
30. J.E. Huheey, E.A. Kieter, R.L. Kieter, Inorganic Chemistry, 4th ed., Dorling Kindersley Pvt. Ltd., India, 2011.
31. A.B.P. Lever Inorganic Electronic Spectroscopy, Elsevier Science Publishing Company, Amsterdam, 1984.
32. R.L. Dutta, A. Syamal, Elements of Magnetochemistry, second edition, Newdelhi, 1993.
33. D.J.E. Ingram, Spectroscopy at Radio and Microwave frequencies, 2nd ed., Butterworth, London.
34. B.S. Garg, M.R.P. Kurup, S.K. Jain, Y.K. Bhoon, Trans.Met. Chem, 1988; 13: 92.
35. S. Stoll, A. Schweiger, J. Magn. Reson, 2006; 178: 42.
36. B. Bleany, R.S. Rubins, Proc. Phys. Soc. Lond, 1961; 77: 103.
37. R. Singh, I.S. Ahuja, C.L. Yadava, Polyhedron, 1981; 1: 327.
38. A. Sreekanth, M. Joseph, H.-K. Fun, M.R.P. Kurup, Polyhedron, 2006; 25: 1408.
39. A.W. Coats, J.P. Redfern, Nature, 1964; 20: 68.
40. O.A.M. Ali, J. Coord. Chem, 2007; 60(11): 1213.
41. D.Y. Sabry, T.A. Youssef, S.M. El-Medani, R.M. Ramadan, J. Coord. Chem, 2003; 56: 1375.
42. K.C. Gupta, H.K. Abdulkadir, J. Macromol. Sci., Part A: Pure Appl. Chem, 2008; 45: 53.
43. N.M. Hosny, Transition Met. Chem, 2007; 32: 117.
44. C. Demetgul, Carbohydr. Polym, 2012; 89: 354.
45. E.L. Wehry, B.W. Rossiter, R.C Baetzold, eds., Physical methods of Chemistry, Wiley, Newyork, 1993; 9.
46. E.L. Wehry, G.G. Guilbault,ed., Practical Fluorescence, 2nd ed., Newyork, 1990.
47. G. Bottiroli, A.C. Croce, P. Balzarini, D. Locatelli, P. Banglioni, P. Lo Nostro, M. Monici, R. Pratesi, Photochem. Photobiol, 1997; 66(3): 374.
48. B. Laura, Talarico, E.B. Damonte, Virology, 2007; 363: 473.